Eur. Phys. J. A **30**, 397–411 (2006)
DOI 10.1140/epja/i2006-10134-5

THE EUROPEAN PHYSICAL JOURNAL A

Spectroscopy and single-particle structure of the odd-Z heavy elements ^{255}Lr, ^{251}Md and ^{247}Es

A. Chatillon[1,a], Ch. Theisen[1,b], P.T. Greenlees[2], G. Auger[3,c], J.E. Bastin[4], E. Bouchez[1], B. Bouriquet[3], J.M. Casandjian[3,d], R. Cee[3], E. Clément[1], R. Dayras[1], G. de France[3], R. de Toureil[3], S. Eeckhaudt[2], A. Görgen[1], T. Grahn[2], S. Grévy[6,e], K. Hauschild[7], R.-D. Herzberg[4], P.J.C. Ikin[4], G.D. Jones[4], P. Jones[2], R. Julin[2], S. Juutinen[2], H. Kettunen[2], A. Korichi[7], W. Korten[1], Y. Le Coz[1,f], M. Leino[2], A. Lopez-Martens[7], S.M. Lukyanov[9], Yu.E. Penionzhkevich[9], J. Perkowski[2,g], A. Pritchard[4], P. Rahkila[2], M. Rejmund[3], J. Saren[2], C. Scholey[2], S. Siem[7,h], M.G. Saint-Laurent[3], C. Simenel[1], Yu.G. Sobolev[9], Ch. Stodel[3], J. Uusitalo[2], A. Villari[3], M. Bender[1,i], P. Bonche[5], and P.-H. Heenen[8]

[1] CEA Saclay, DSM/DAPNIA/SPhN, F-91191 Gif-sur-Yvette Cedex, France
[2] University of Jyväskylä, Department of Physics, P.O. Box 35, FIN-40014, Finland
[3] GANIL, Boulevard Henri Becquerel, B.P. 55027, F-14074 Caen Cedex 5, France
[4] Oliver Lodge Laboratory, Department of Physics, University of Liverpool, Liverpool L69 7ZE, UK
[5] CEA Saclay, DSM/SPhT, F-91191 Gif-sur-Yvette Cedex, France
[6] LPC, 6 boulevard du Maréchal Juin, F-14050 CAEN Cedex, France
[7] CSNSM, Bat. 104-108, F-91405 Orsay, France
[8] Service de Physique Nucléaire Théorique, Université Libre de Bruxelles, C.P. 229, B-1050 Bruxelles, Belgium
[9] Joint Institute for Nuclear Research, 141980, Dubna, Russia

Received: 20 July 2006 / Revised: 20 September 2006 /
Published online: 24 November 2006 –
Communicated by J. Äystö

Abstract. The odd-Z isotope ^{255}Lr, its daughter ^{251}Md and grand-daughter ^{247}Es were studied in two experiments performed at GANIL and the University of Jyväskylä. The ^{255}Lr nuclei were produced using the cold fusion-evaporation reaction ^{209}Bi(^{48}Ca, 2n)^{255}Lr at a bombarding energy of 217 MeV. The single-particle structure and decay properties were investigated using α, γ and electron spectroscopy. The ground-state spin and parity could be assigned for ^{255}Lr $(1/2^-)$ and ^{251}Md $(7/2^-)$. States corresponding to the $7/2^+[633]$, $7/2^-[514]$ and $1/2^-[521]$ Nilsson orbitals were observed. Results are compared to experimental data obtained in neighbouring isotopes and to Hartree-Fock-Bogoliubov calculations using the Skyrme interaction SLy4 and a density-dependent pairing interaction. The position of the $1/2^-[521]$ orbital from the spherical $2f_{5/2}$ shell is discussed.

PACS. 27.90.+b $220 \leq A$ – 23.60.+e α decay – 23.20.Lv γ transitions and level energies – 23.20.Nx Internal conversion and extranuclear effects

1 Introduction

The study of super-heavy elements and the quest to find the predicted island of stability is a fertile topic of nuclear-structure physics. Nuclei above $Z = 104$, the transactinide elements, would be unstable against fission without stabilising shell effects. They are therefore very fragile objects, which seriously complicates experimental studies. Due to very low-production cross-sections (at the level of pb or lower) only the basic properties of the heaviest elements can be deduced, such as decay channel, α-decay energy or lifetime. For a review of work on the heaviest elements,

[a] *Present address:* Gesellschaft für Schwerionenforschung mbH, D-64220 Darmstadt, Germany.
[b] e-mail: christophe.theisen@cea.fr
[c] *Present address:* Collège de France, 11 place M. Berthelot, F-75231 Paris Cedex 5, France.
[d] *Present address:* CEA Saclay, DSM/DAPNIA/SAP, F-91191 Gif-sur-Yvette Cedex, France.
[e] *Present address:* GANIL, Boulevard Henri Becquerel, B.P. 55027, F-14074 Caen Cedex 5, France.
[f] *Present address:* CEA Cadarache, F-13108 St Paul lez Durance Cedex, France.
[g] *Present address:* Department of Physics and Radiation Safety, University of Lodz, Poland.
[h] *Present address:* Department of Physics, Oslo University, 0316 Oslo, Norway.

[i] Work performed in the framework of the ENST (Espace de Structure Nucléaire Théorique).

see *e.g.* [1]. On the theoretical side, there is still a debate concerning the position of the island of stability that is expected for super-heavy elements as theoretical models give conflicting predictions for the shell closure depending on the chosen effective mean-field interaction, see *e.g.* [2–4]. The uncertainties in the models are also reflected in the region of the heaviest actinides ($Z < 104$), also known as the transfermium region, where experimental studies are made easier since the production cross-sections are much higher, at the level of μb. The study of transfermium elements is a step towards improved knowledge for the heaviest elements: the deformed region around $N = 152$ and $Z = 100$ can be considered as a viewpoint towards the super-heavy island of stability.

A breakthrough in prompt γ and electron spectroscopy emerged a few years ago with the availability of highly efficient experimental devices [5,6]. The collective rotational ground-state band of ^{254}No, first observed at Argonne [7] and then at the University of Jyväskylä (JYFL) [8,9], is now established as a textbook example. Besides γ-ray spectroscopy, prompt electron spectroscopy [10] and K-isomeric [11,12] states have been studied. Collective properties near the $N = 152$, $Z = 100$ deformed shell gap have also been studied in the even-even nuclei ^{250}Fm [13] and ^{252}No [14]. With the recent improvement in detection efficiencies, prompt spectroscopy of the odd-mass nuclei ^{251}Md [15], ^{253}No [16,17] and ^{255}Lr [18] has been performed, providing more insight into single-particle structure.

Together with the collective properties, the study of single-particle states in odd-mass nuclei provides crucial complementary information. Alpha-decay experiments are well suited for such studies since this mode is very sensitive to the initial- and final-state wave functions. Often it is possible to establish the spin and parity of not only the ground state, but also of the first excited states. The study of single-particle states and the comparison with theoretical models is the goal of these experiments, but there is also hope to pin-down high-lying orbitals from the super-heavy element region, which approach the Fermi level in the transfermium region as the deformation increases. Although α-decay of the heaviest elements has been studied from the beginning of super-heavy element production, in most cases the level schemes that can be established are far from comprehensive [1,5,6]. Detection of γ and electron transitions following the α-decay are mandatory tools to complete level schemes, as these allow the multipolarities of the transitions to be determined. Such devices, combining α, electron and γ spectroscopy have been developed recently. Examples are GREAT [19] built by a group of U.K. Universities and sited at JYFL, BEST at GANIL (this work) and GABRIELA [20] at Dubna.

This study focuses on the odd-Z transfermium nucleus ^{251}Md, produced following the α-decay of ^{255}Lr. Although particular emphasis was placed on $^{251}_{101}$Md, the mother nucleus $^{255}_{103}$Lr and its grand-daughter $^{247}_{99}$Es have been studied using genetic correlations. Such correlations allow the level scheme and decay path to be determined for the whole decay chain from ^{255}Lr down to ^{247}Es. First synthesized in the 1970s [21], ^{251}Md is particularly poorly known. Based on mass systematics and ^{255}Lr α-decay fine structure, two excited states have been suggested [22], for which there is no strong experimental basis. A ground-state spin and parity of $7/2^-$ has been recently suggested [23].

This paper reports on two experiments dedicated to the study of the α-decay of ^{255}Lr. In the next section, the experimental devices and conditions will be described. The experimental results concerning the α, electron and γ-decay will be presented in sects. 3, 4 and interpreted in sect. 5. Comparison with neighbouring nuclei and theory, along with the consequences for single-particle structure in the transfermium region will be discussed in sect. 6.

2 Experimental techniques

Two experiments aimed at the study of the ^{255}Lr decay have been performed at JYFL and at GANIL, Caen. As will be shown in this section, the complementary performances of both devices were a benefit. At JYFL, a better α energy resolution was obtained while the electron energy resolution and gamma-ray detection efficiency were improved at GANIL. In both experiments, the ^{255}Lr nuclei were populated using the cold fusion-evaporation reaction ^{209}Bi(^{48}Ca, 2n)^{255}Lr.

2.1 Experiment at the University of Jyväskylä

Eight ^{209}Bi targets having a thickness of 400–440 μg/cm^2 were installed on a rotating wheel and bombarded by a ^{48}Ca^{10+} beam accelerated to an incident energy of 221 MeV by the JYFL $K = 130$ cyclotron. An average beam intensity of 800 enA was obtained for the duration of the experiment. At the beginning of the experiment, an excitation function was measured using a set of C degrader foils. Optimum production of ^{255}Lr was found for a center-of-target energy of 217 ± 2 MeV. At this energy, contamination by the 1n channel (^{256}Lr) is expected to be less than 4% [24]. Fusion-evaporation products were separated from the beam and the large background of parasitic reactions such as fission, transfer and elastic scattering by the RITU gas-filled separator [25]. RITU was filled with He gas at a pressure of 0.6 mbar to obtain an average equilibrium recoil charge state. A transmission of approximately 35% is estimated for the ^{48}Ca + ^{209}Bi reaction. Recoiling nuclei and their subsequent decay were detected at the focal plane of RITU using an early implementation of the GREAT spectrometer [19]. GREAT consists of a Multi-Wire Proportional Counter (MWPC) gas detector placed 20 cm upstream of two Double-Sided Silicon Strip Detectors (DSSSD); the time of flight being measured between the MWPC and the DSSSD. Each DSSSD has a size of 60×40 mm^2, and is of 300 μm thickness with 60 vertical and 40 horizontal strips. An average energy resolution of approximately 25 keV for 8 MeV α-particles was obtained. An internal α calibration was performed on-line using known activities produced through reaction of the ^{48}Ca beam with a ^{172}Yb target. Escaping α-particles were

detected by a "box" of 28 pin-diodes placed around the two DSSSDs. The signals from each detector were processed independently and time-stamped to a resolution of 10 ns by the trigger-less Total Data Readout (TDR) acquisition system [26]. Events were reconstructed in software and the data analysed using the GRAIN [27] package. During a total irradiation time of 135 hours, a total of around 6000 ^{255}Lr α-decays were observed.

2.2 Experiment at GANIL

The $^{48}Ca^{8+}$ beam was accelerated by the CSS1 cyclotron, and a beam energy of 219.4 MeV was measured in the "alpha" spectrometer. This energy corresponds to a center-of-target energy of 217.1 MeV, which was chosen to fit with the maximum of the excitation function for the 2n channel [24] as in the previous experiment. An average beam intensity of $\sim$ 1000 enA was delivered during the irradiation. The LISE spectrometer [28] in its FULIS configuration [29] was used to select the ^{255}Lr recoils. Eighteen ^{209}Bi targets, with thicknesses of 400–460 μg/cm^2 were installed on a rotating target wheel having a radius of 30 cm and a speed of 1500 r.p.m. The beam structure was synchronized to the wheel rotation. Behind the ^{209}Bi targets eighteen 35 μg/cm^2 C charge-reset foils were installed on a second wheel placed 15 cm downstream. The target quality was continuously monitored using a Si and a BaF2 detector. In addition, the target wheel position was recorded in order to associate it with focal-plane events. Recoil products were separated from the background using the LISE Wien Filter [30] which was preceded and followed by a quadrupole triplet. The ion-optical settings were optimized using the Zgouby [31] and COSY Infinity [32] packages. A velocity of 0.52 cm/ns was selected using a Wien Filter field combination of $E = 150$ kV/m and $B = 3.1\ 10^{-2}$ T. It should be noted that the electric field is reduced by approximately 10% compared to a perfect Wien Filter value due to a slight asymmetry. A transmission efficiency of around 15% and a beam rejection factor of 2×10^{10} were measured. The primary beam (shifted upward) was stopped in the middle of the Wien Filter by a water-cooled Cu shield. Additional slits at the mid-filter were used to further reduce the background. Recoil products were detected at the focal plane using a "galotte" detector and a DSSSD. The DSSSD had dimensions of 50×50 mm^2, with 48×48 strips and a thickness of 300 μm. The "galotte" detector was used to measure the time-of-flight with respect to the implantation DSSSD. The "galotte" consists of a mylar foil for electron emission and a micro-channel plate detector. The cooled DSSSD was also used to detect α-particles with an energy resolution of around 40 keV for 8 MeV α-particles. Known activities from the reaction ^{176}Yb(^{48}Ca, xn)$^{224-x}$Th were used to perform an internal calibration. A tunnel of four four-fold segmented cooled Si detectors with dimensions 50×50 mm^2 and 1 mm thickness was used to detect escaping α-particles and conversion electrons. This "tunnel" array of Si detectors is known as BEST (Box for Electron Spectroscopy after Tagging). An energy resolution of 7–10 keV was obtained for electrons with an energy of 320 keV. The efficiency of BEST was simulated using the GEANT 4 package [33], taking into account the measured ^{255}Lr recoil distribution in the DSSSD. An efficiency of 15% at an electron energy of 200 keV was deduced. BEST was surrounded by four segmented germanium detectors provided by the EXOGAM [34] Collaboration. GEANT 4 simulations were also performed to estimate the γ-ray detection efficiency. The full geometry of the BEST array, along with the ^{255}Lr implantation distribution was included. A maximum efficiency of $\sim$ 22% at 120 keV was found. It should be noted that GEANT 4 is known to have an accuracy of around 10% for γ-ray efficiency simulations. Events were time-stamped using 100 kHz CAMAC and 100 MHz VXI clocks. Data were analysed using the ROOT package [35]. The trigger for the data acquisition system was provided by the implantation (DSSSD) or tunnel (BEST) detectors. During an irradiation time of 142 hours, a total of around 6000 ^{255}Lr α-decays were measured.

3 Alpha-decay

In order to reduce the background from low-energy implantation events in the region of expected α-decays, anti-coincidences between the DSSSD and the time-of-flight detector (the "galotte" at GANIL; the MWPC at JYFL) were demanded before the α-decay spectrum was incremented. Examples are shown in figs. 1, 2(a), where α-decay lines from ^{255}Lr, the daughter nucleus ^{251}Md, and from ^{255}No which is populated via the electron capture or β-decay of ^{255}Lr are observed. The peak marked ^{211}Po is due to the decays of long-lived activities produced in the calibration runs with the ^{172}Yb (JYFL) or ^{176}Yb (GANIL) targets.

Using genetic correlations, whereby events are searched for which occur at the same position in the DSSSD within a certain time window, the ^{255}Lr and ^{251}Md α-decays can be isolated. Figures 1, 2(b) show the spectra of α-decay events correlated to recoils within a search time of 2 minutes. These spectra are dominated by the decay of ^{255}Lr, with the presence of a small contribution due to the decay of ^{255}No. Some of the ^{255}No decays are correlated to recoils as the β-particle emitted deposits little energy in the DSSSD and is not registered. No charged particles are emitted during the electron capture process. Figures 1, 2(c) correspond to recoil-α-α correlations using a maximum search time of two minutes between the recoil and the first α-decay, and 20 minutes between the mother and daughter α-decays. Due to accidental correlations, a small contribution from the decay of ^{255}Lr persists. Recoiling fusion-evaporation products are identified by setting a two-dimensional gate on the recoil energy *versus* time-of-flight matrix: see fig. 3. In the genetic correlation analysis, no α energy condition was applied. In the following two subsections, the α-decay properties of ^{255}Lr and ^{251}Md determined from the data will be detailed.

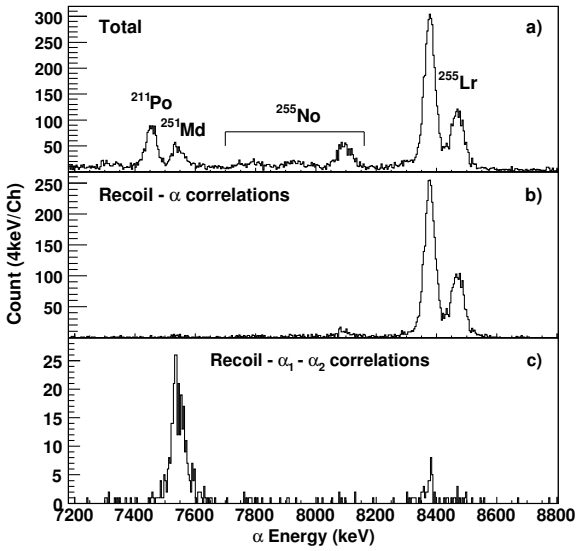

Fig. 1. Example of α-decay spectra obtained in the GANIL experiment. a) Total α-decay spectrum, b) result of recoil-α correlations, c) result of recoil-α-α correlations (second generation).

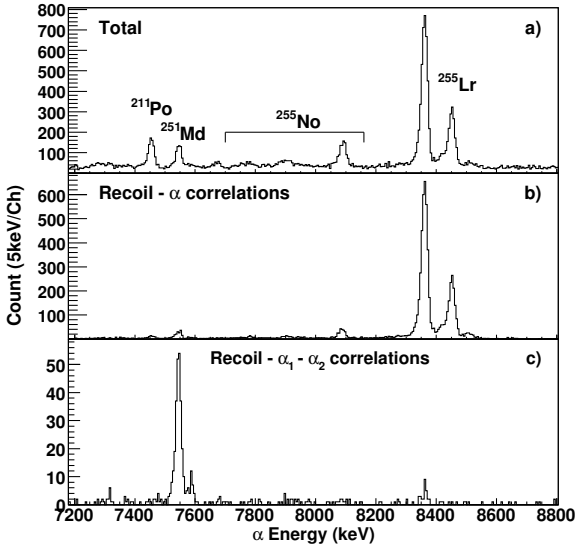

Fig. 2. Same as fig. 1, but for data obtained at JYFL.

3.1 The α-decay of ^{255}Lr

Figure 4 shows an expanded region of the spectrum of α-decays correlated to recoil events. Since the energy resolution achieved in the experiment at JYFL was better than that in the GANIL experiment, the energies obtained in the former are adopted. As is shown from the fit in fig. 4, five peaks at energies of 8290, 8365, 8420, 8457 and 8512 keV can be separated. The fit is performed by first fixing the peak shape parameters using an α-decay line

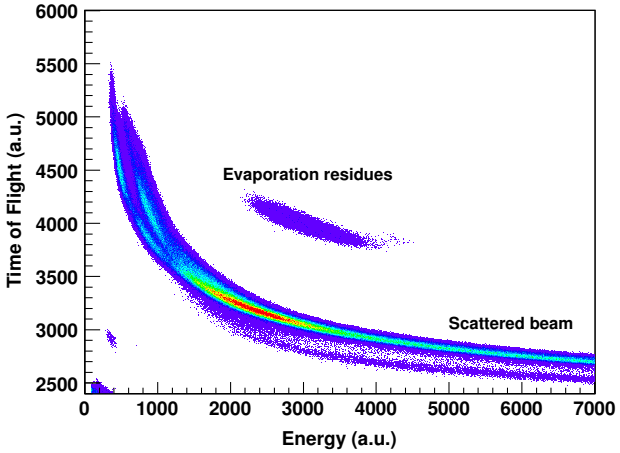

Fig. 3. Time of flight between the "galotte" and the implantation detector as a function of the implantation energy (GANIL experiment).

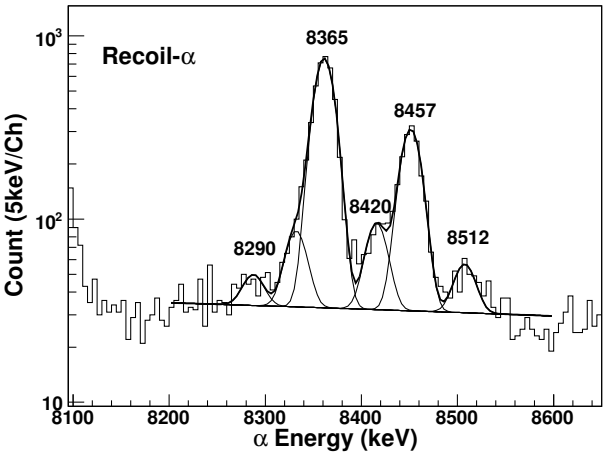

Fig. 4. Portion of the α-decay spectrum, resulting from recoil-α correlations, in the ^{255}Lr region. Data are taken from the JYFL experiment.

from the calibration data. Lifetime plots for the decays are obtained from the time difference, Δt, between the α-decay and the recoil implantation. The extracted lifetimes are adjusted using the function:

$$f(\Delta t) = ae^{-(\lambda+r)\Delta t} + be^{-r\Delta t}, \quad (1)$$

where λ is the decay constant of the state, and r is a component which arises due to random correlations [36].

3.1.1 The 8365 keV α-decay

This decay was previously identified [37,38] as the decay from the ground-state of ^{255}Lr and determined to have a half-life of 22 ± 5 s. The decay curve for this peak is shown in the upper panel of fig. 5. In the inset is an expansion of the early part of the curve, which shows that the decay is characteristic of a growth decay process. This indicates

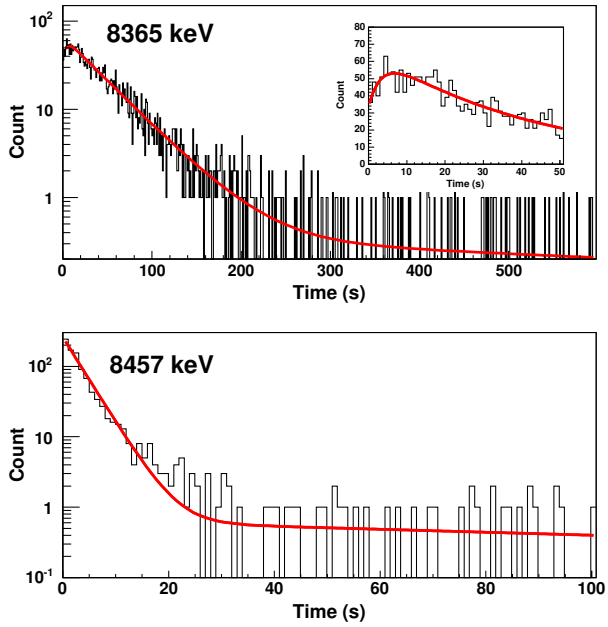

Fig. 5. Decay curves corresponding to the 8365 keV (upper panel) and 8457 keV (lower panel) α-decay lines.

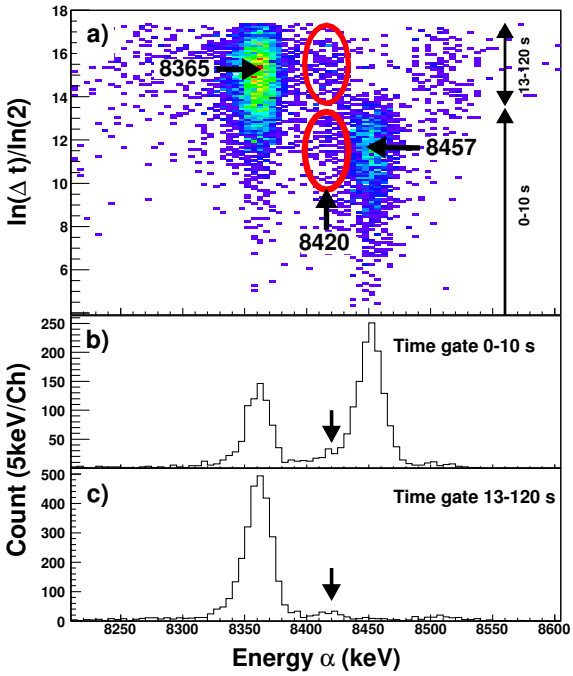

Fig. 6. a) Plot of $\ln(\Delta t)/\ln(2)$, Δt being expressed in ms, as a function of the α-particle energy. The two decay components of the 8420 keV transition are enclosed in the two ellipses. b) and c) alpha spectra obtained using two Δt conditions shown in panel a). The arrows indicate the 8420 keV line.

that the decaying state is fed by an isomer. In this particular case, the curve is fitted with the function

$$f(\Delta t) = a\{e^{-(\lambda_2+r)\Delta t} - e^{-(\lambda_1+r)\Delta t}\} + be^{-(\lambda_2+r)\Delta t} + ce^{-r\Delta t}, \quad (2)$$

where λ_2 (λ_1) is the decay constant of the isomer (α-decaying state). Decay half-lives of $T_{1/2}(8365) = 31.1 \pm 1.3$ s and $T_{1/2}(\text{isomer}) = 2.3 \pm 1.0$ s are deduced for the 8365 keV α-decay and feeding isomeric decay, respectively. This line is interpreted as corresponding to the ground-state decay of ^{255}Lr. The ratio of the isomeric state to feeding from other branches can be calculated from the coefficients of eq. (2). Assuming negligible β or E.C. branches from the isomeric state, we deduce a ratio of 0.94 ± 0.44 *i.e.* $48 \pm 12\%$ of the ground-state feeding proceeds via the isomeric state.

3.1.2 The 8457 keV α-decay

Evidence for this decay was first given by Eskola *et al.* [37] and later confirmed by Bemis *et al.* [38]. In these two references, the 8365 keV and 8457 keV decays were deduced to have the same half-life (22 ± 5 s). The decay curve of the 8457 keV line is shown in the lower panel of fig. 5, from which a half-life of 2.53 ± 0.13 s is deduced. This corresponds well to the deduced half-life of the isomer feeding the ground state (see sect. 3.1.1). The initial state of the 8457 keV transition is interpreted as corresponding to a 2.53 s isomer in ^{255}Lr, feeding partially the ground state.

3.1.3 The 8420 keV α-decay

The decay curve of this α line shows two components with half-lives of 2.8 ± 0.6 and 30 ± 4 s, consistent with the half-lives of the 8365 keV (31.1 s) and 8457 keV (2.53 s) lines. The two components can be clearly seen in a two-dimensional plot of α-decay energy (E_α) against the logarithm of the decay lifetime ($\ln(\Delta t)$), as shown in fig. 6. The number of events in the 8420 keV doublet constitutes 5.7% of the total number of events attributed to the decay of ^{255}Lr (data from JYFL), with a contribution of $37 \pm 10\%$ ($63 \pm 10\%$) from the 2.8 s (30 s) component. A small contribution from the 8430 keV transition of ^{256}Lr, which has a lifetime of 27 s [37,38], cannot be excluded. However, an 11% population of ^{256}Lr compared to ^{255}Lr would be required to explain the intensity of the 30 s component (JYFL data), which can be excluded. Moreover, the peak is present in recoil-α-α correlations, the statistics compared to the recoil-α–gated spectrum being compatible with a ^{255}Lr assignment. The half-life could not be deduced from the GANIL data as the α energy resolution is not sufficient. It should be noted, however, that the same intensity is obtained for the full 8420 keV peak. Since the beam energy is measured very precisely, and since evidence for other ^{256}Lr peaks was not found, this again excludes a significant contamination. However, as a precaution, the 30 s 8420 keV intensity should be taken as an upper limit.

As shown in figs. 6(b,c), the 8420 keV line is present using two different correlation times corresponding to "slow" and "fast" components. The possibility that the 2.8 s com-

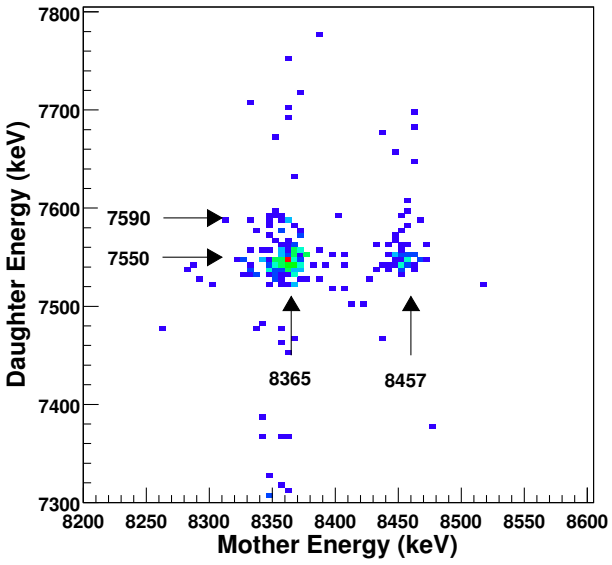

Fig. 7. Alpha-alpha correlation matrix. A search time of 15 (3) minutes has been used for the daughter (mother) decay. Data are taken from the JYFL experiment.

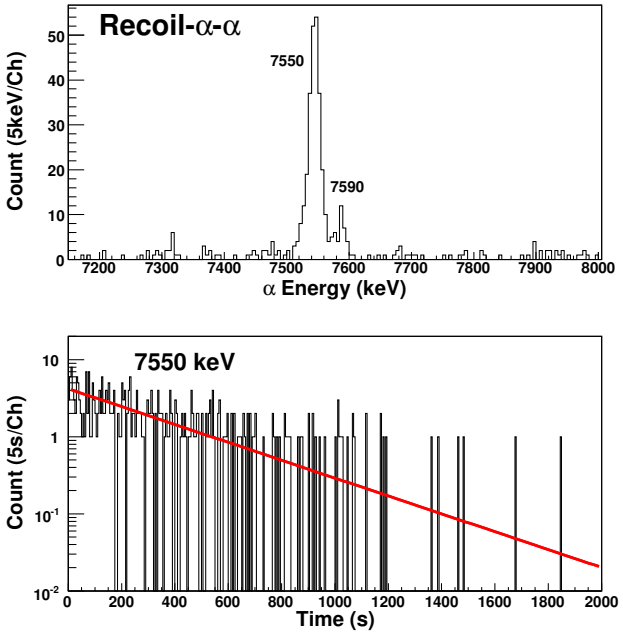

Fig. 8. Upper panel: alpha-decay spectrum of ^{251}Md resulting from recoil-α-α correlations. Lower panel: time distribution for the 7550 keV α-decay. Data are taken from the JYFL experiment.

ponent corresponds to a tail of the 8457 keV line due to the detector response can be ruled out, as it would be expected to observe such a tail for all α-decay lines. This is not observed in the JYFL data set where the detector resolution was superior. As will be discussed in more detail in sect. 5.2, the 2.8 s component is interpreted as resulting from a summing effect.

It is therefore concluded that the 8420 keV transition is a doublet; the initial decaying states being either the ^{255}Lr ground state or the 2.53 s isomeric state.

3.1.4 The 8290 keV α-decay

An α-decay with an energy of 8290 keV was observed with low statistics in both the GANIL and JYFL experiments with an half-life of approximately 35 s. The assignment of this transition remains uncertain, though the decay appears in recoil-α-α correlations which suggests that it originates from ^{255}Lr.

3.1.5 The 8512 keV α-decay

The α-decay with an energy of 8512 keV is observed at JYFL with an half-life of 87 ± 40 s and is not correlated to the α-decay of ^{251}Md. It has not been observed at GANIL. It is therefore not assigned to the α-decay of ^{255}Lr.

3.2 The α-decay of ^{251}Md

The spectrum of α-decays corresponding to the second generation of genetic correlations (see the upper panel of fig. 8), displays two peaks with energies of 7550 and 7590 keV. Search times of up to 3 minutes for the first generation and 15 minutes for the second generation of decays were used. The analysis of mother-daughter α correlations shows that these two peaks are correlated with the ^{255}Lr decay: see fig. 7. The 7590 keV line is deduced to be due to the effects of conversion electron summing, and will be discussed further in sect. 4.1. The 7550 keV line was previously observed and assigned to ^{251}Md by Eskola [21].

3.2.1 Half-life

The decay curve corresponding to the 7550 keV α-decay is presented in the lower panel of fig. 8. Search times of up to 4 minutes for the first generation of α-decays and 40 minutes for the second generation have been used. Since the random contribution is negligible using recoil-α-α correlations, the time distribution has been fitted using a single exponential. A decay half-life of 4.27 ± 0.26 min is deduced from the combined JYFL and GANIL data. Although the statistics for the 7590 keV line were limited, a lifetime of 4.3 ± 0.6 min could be extracted. The initial state of the two peaks is therefore the same, *i.e.* the ground state of ^{251}Md.

3.2.2 Alpha-decay branching ratio

The ^{251}Md α-decay branching ratio can be deduced by comparing the intensities of the ^{255}Lr peaks in recoil-α-α and recoil-α correlations. A correction for the relevant search times and the α-particle detection efficiency

Table 1. Summary of the α-decay properties of ^{255}Lr and ^{251}Md.

Isotope	Energy (keV)	Intensity (%)	Half-life	Q_α (keV)	H.F.	α branching ratio (%)
^{251}Md	7550(1)	87 ± 3	4.27 ± 0.26 min	7672(1)	1.4	10(1)
	7590(5)[a]	13 ± 3	4.3 ± 0.6 min	–	14	
	7550(1) sum	100	4.27 ± 0.26 min	7672(1)	1.3	
^{255}Lr	8290(5)[b]	1.2 ± 0.4	~ 35 s	–	–	85 (from [22])
	8365(2)	67.1 ± 1.5	31.1 ± 1.3 s	8498(2)	1.8	
	8420(10)	$\leq 3.6 \pm 0.5$	30 ± 4 s	8554(10)	≥ 52	
	8420(10)[a]	2.1 ± 0.5	2.8 ± 0.6 s	–	3[c]	
	8457(2)	26.0 ± 0.8	2.53 ± 0.13 s	8592(2)	≥ 0.6[d]	

[a] Interpreted as a line resulting from summing.
[b] Tentative assignment.
[c] Assuming an α energy of 8322 keV without summing.
[d] Possible low-energy tail due to summing.

($\epsilon_\alpha = 55\%$) are included in the calculation. The branching ratio (BR) could be deduced for the sum of the 7550 and 7590 keV transitions, correlated to either the 8365 or 8457 keV α-decay in ^{255}Lr. The values obtained are:

$$\mathrm{BR(Md, Lr(8365))} = 9.3 \pm 0.9\%, \quad (3)$$
$$\mathrm{BR(Md, Lr(8457))} = 10.9 \pm 1.5\%. \quad (4)$$

The similar value obtained when correlating with one of the two strongest ^{255}Lr α-decays shows that either the final state in ^{251}Md is the same (*i.e.* the ground state), or that the ^{255}Lr α-decays feed two different states connected by an electromagnetic transition.

3.3 Summary of α-decay properties

A summary of the α-decay properties of ^{255}Lr and ^{251}Md is given in table 1. A larger uncertainty for the 8420 keV line is quoted as this doublet could not be clearly resolved. The Hindrance Factor (H.F.) corresponds, for a given initial state, to the ratio of the experimental partial α-decay half-life to the half-life calculated using a barrier penetration model described in [39] including a screening effect described in [40]. Its value is close to unity when the initial- and final-state wave functions are similar, and increases as the wave functions differ, in particular with a change of parity or for spin-flip transitions.

In ^{255}Lr, two α-decaying states have been observed, as discussed above. The ground state, having a half-life of 31.1 s, decays via two α transitions with energies of 8365 and 8420 keV, and by electron capture decay to ^{255}No. The electron-capture probability of 15% given in [22,37] is compatible with our experimental data. An isomeric state, with a half-life of 2.53 s decays by two α transitions with energies of 8420 and 8457 keV, and by an electromagnetic transition feeding the ground state. Assuming a negligible beta decay or electron capture probability for this isomeric state, the ratio of the ground-state feeding to the α-decay branches is calculated to be 1.5. The 8290 keV line is tentative. Note that we have not found evidence in ^{255}Lr for a spontaneous fission branch. The values obtained will be discussed in sect. 5.

4 Coincident γ-ray and electron spectroscopy

4.1 Alpha-γ spectroscopy

The germanium detectors surrounding the implantation DSSSD detectors can be used to detect γ-rays in prompt coincidence with any detected α-particles. A matrix corresponding to prompt α-γ correlations is presented in the upper panel of fig. 9. No prompt coincidences with α-decays assigned to ^{255}Lr are observed, which indicates that the states fed in ^{251}Md either decay by highly converted transitions, or are isomeric. Coincidences between α-decays of ^{251}Md and γ-rays from ^{247}Es are indicated by circles drawn with a solid line. A projection from the matrix, produced by gating on the ^{251}Md α-decay line is shown in the lower panel of fig. 9, where two new transitions with energies of 243 and 293 keV are clearly seen. Weaker evidence for a γ-ray transition at 180 keV is also found.

At first sight, both the 243 and 293 keV transitions are correlated to the ^{251}Md 7550 keV α-decay. However, α-particle spectra gated on the 243 and 293 keV γ-rays show small differences, as can be seen in fig. 10. The α-particle spectrum gated by the 243 keV transition (fig. 10(d)) is shifted to higher energy by approximately 40 keV compared to the α-particles in coincidence with the 293 keV transition (fig. 10(c)). The 40 keV difference can be explained assuming an highly converted 50 keV transition (*i.e.* 293-243 keV) in coincidence with the 243 keV transition. The internal conversion electrons and associated X-rays, Coster-Kronig or Auger electrons are emitted in coincidence with the 7550 keV α line and their energies are summed in the implantation detector.

To lend weight to this interpretation, GEANT 4 simulations of the summing effect have been carried out. It is assumed that the recoils are implanted at a depth of 10 μm, and that the transition has an energy of 50 keV and multipolarity $M1$. This leads to an average conversion electron energy of 27 keV which is almost fully absorbed in the Si detector. The emission of L or M X-rays following conversion was included in the simulation, taking into account the relevant X-ray fluorescence yields and intensities

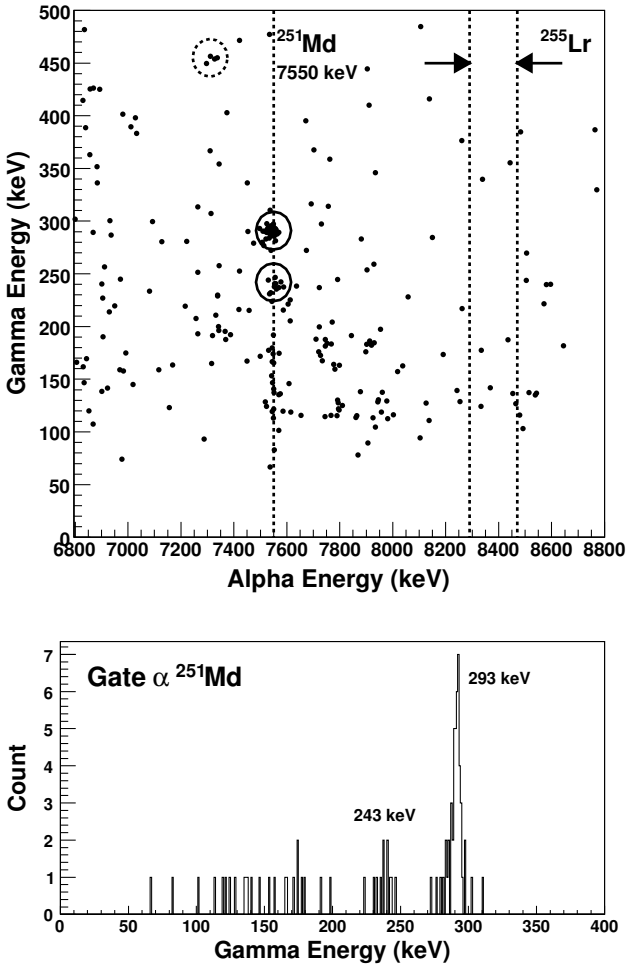

Fig. 9. Upper panel: matrix corresponding to prompt α-γ correlations. Lower panel: γ transition in coincidence with the ^{251}Md α line. Data are taken from the GANIL experiment.

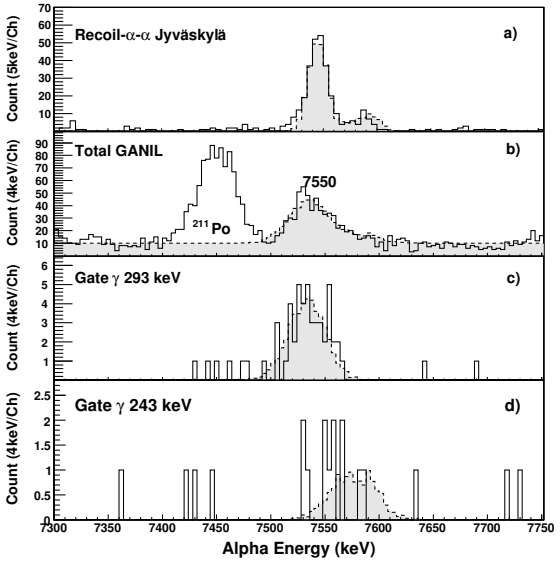

Fig. 10. α-particle energy spectrum resulting from recoil-α-α correlation taken from JYFL (a). Total α-particle energy spectrum taken from GANIL (b). The α-particle energy spectrum in coincidence with the 293 keV or 243 keV γ-rays is shown by solid lines in panels (c) and (d), respectively. The result of the GEANT 4 simulations (see text for explanation) are shown shaded in grey.

per shell vacancies [41]. Since experimental information for Auger yields and energies in very heavy nuclei is not available, a simplified LMM and LMN Auger electron emission has been implemented. Remaining Coster-Kronig and MXY Auger electrons were included as a single emission since this contribution has a sum energy less than 10 keV and is fully absorbed in the implantation detector. Taking into account the uncertainties in the different processes (for instance, the $L1$ shell fluorescence yield uncertainty is 20% [41]), only qualitative comparisons between the experimental spectra and the simulations can be made. The results of the simulations are shown in grey in fig. 10. It can be seen that the simulations reproduce satisfyingly the experimental data: a summing energy of 43 keV is simulated compared to an experimental value of 40 keV. Finally, the intensity ratio $I_\alpha(7550)/I_\alpha(7590) = 6.7 \pm 2$ is consistent with the ratio $I_\gamma(293)/I_\gamma(242) = 4.4 \pm 2$.

The 7590 keV line is therefore not a new α-decay from ^{251}Md, but results from the summing of conversion electrons and X-rays, Coster-Kronig or Auger electrons. A similar summing effect has also been observed in several experiments: see, *e.g.* [23,42]. The simulation will not change drastically if multipolarities other than $M1$ are assumed for the 50 keV transition as at this energy internal conversion occurs mainly from the L shell. However, transitions with $\Delta l > 2$ can be excluded as their lifetime would be too long to give a summing effect with the α-particles. The multipolarity of the 50, 243 and 293 keV transitions will be discussed in sect. 4.3.

In the upper panel of fig. 9, the dashed circle highlights a coincidence between 7330 keV α-particles and a 452 keV γ-ray transition. The 7330 keV α is due to the decay of ^{255}Md and this observation confirms a previous measurement [43]. ^{255}Md is populated after successive electron captures from ^{255}Lr via ^{255}No.

4.2 Alpha-electron spectroscopy

The silicon detectors surrounding the DSSSD implantation detector can be used to detect conversion electrons emitted from the decay of states populated by α-decay. A matrix corresponding to prompt α-electron coincidences is presented in fig. 11. Conversion electrons in coincidence with the ^{255}No α-decay are clearly observed, which shows the validity of the experimental technique.

No evidence for electrons in coincidence with the ^{251}Md α-decays can be seen. This lack of coincidences is not a negative result, as it allows information concerning the states fed by the α-decays to be inferred. Moreover, the absence of coincident conversion electrons will be used in the next section to constrain the multipolarity of the 293 and 243 keV transitions.

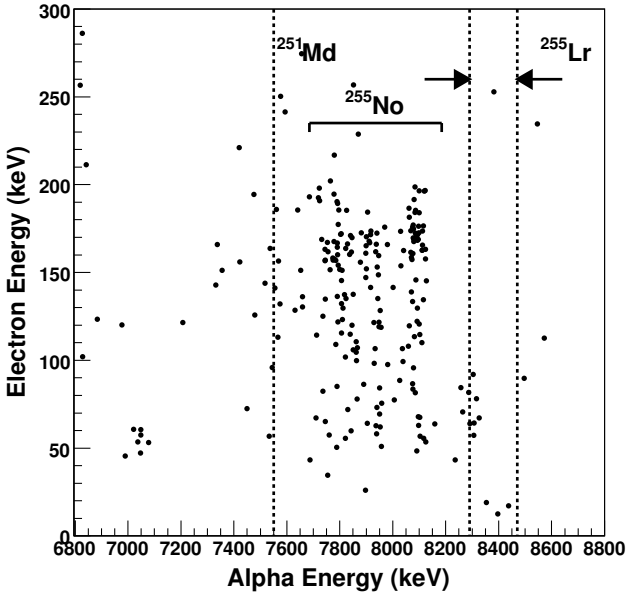

Fig. 11. Matrix of prompt α-electron coincidences. Data are taken from the GANIL experiment.

Nine electron counts with an average energy of 75 ± 10 keV are observed in coincidence with the 8290 keV peak. This distribution is compatible with the conversion of an $E2$, $M1$ or $M2$ transition at 105 ± 10 keV. Therefore, part of the 8290 keV energy should correspond to X-ray summing.

4.3 Multipolarity of the γ-ray transitions

As shown in sect. 4.1, two γ-ray transitions with energies of 243 and 293 keV have been observed in ^{247}Es, in prompt coincidence with the 7550 keV α-decay of ^{251}Md. The multipolarity of the transitions can be deduced from the number of counts in the electron spectrum obtained in coincidence with the same α transition. This spectrum is not shown here, but includes 8 counts, all below 200 keV. It should be noted that some of the counts may correspond to background since the γ-ray efficiency for a 1 mm thick Si detector in which Compton scattering occurs is not negligible. Assuming $E1$, $E2$, $M1$ or $M2$ character for the 293 keV transition, the number of counts due to conversion electrons should be 2, 15, 100 or 300, respectively. These estimates take into account the BEST and clover detector efficiencies. The 293 keV transition is therefore assumed to have $E1$ character. Note that X-rays do not allow $E1$ or $E2$ character to be distinguished as the expected number of counts in the $K_{\alpha,\beta}$ lines is below statistical significance in both cases (1 and 6, respectively) while L X-rays are below the detection threshold.

Similar analysis for the 243 keV transition suggests that the number of counts in the electron peaks should be 1, 6, 33 or 110 for $E1$, $E2$, $M1$ or $M2$ transitions, which rules-out an $M1$ or $M2$ character.

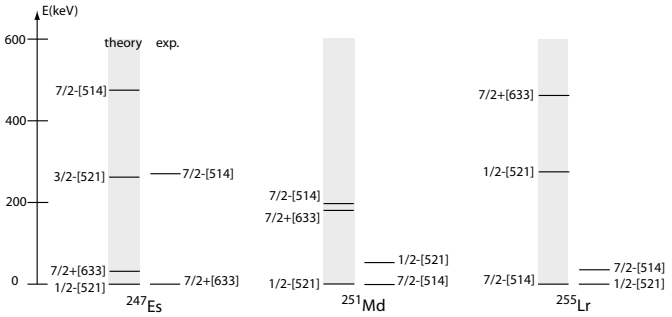

Fig. 12. Comparison between experimental and theoretical level schemes for ^{247}Es, ^{251}Md and ^{255}Lr.

5 Interpretation of the experimental data

Low-lying states have been previously identified in neighbouring Es, Md and Lr isotope, see the discussion in refs. [6,23]. The same single-particle states observed in neighbouring isotopes and predicted by theoretical models are expected to be identified in ^{247}Es, ^{251}Md and ^{255}Lr. We have performed Hartree-Fock-Bogoliubov (HFB) calculations for these 3 isotopes using the Skyrme interaction SLy4 [44] in connection with a density-dependent pairing interaction. The same formalism as in ref. [45] is used. Level schemes obtained by constructing the lowest one–quasi-particle proton excitations are shown in fig. 12. The same quasi-particle levels are found at low energy using the Strutinsky method with a Woods-Saxon [46,47] potential or in HFB calculations performed with a Gogny force [48], but with a different level ordering. Comparison between the deduced experimental and theoretical level schemes will be made in sect. 6.

5.1 ^{247}Es

For ^{247}Es our HFB calculations predict a $1/2^-$ ground state nearly degenerate with a $7/2^+$ level, a $3/2^-$ and a $7/2^-$ level lying below an excitation energy of 500 keV, see fig. 12. In a previous work [49], the ground state of ^{247}Es was assigned to have a $7/2^+$ spin, although a $3/2^-$ spin cannot be excluded (see the discussions in [6,23]).

As discussed in the previous section, the strongest γ-ray transition has an energy of 293 keV and is most likely an $E1$.

Among the four lowest states ($1/2^-$, $7/2^+$, $3/2^-$ and $7/2^-$) predicted by our calculation, an $E1$ transition can only occur between the $7/2^-$ and $7/2^+$ states. The 293 keV transition can therefore be interpreted as the decay from the $7/2^-$ to the $7/2^+$ level which has been tentatively assigned to the ground state [49]. As discussed in the previous sections, the 243 keV γ-ray is most likely an $E2$ or an $E1$ transition. It is also detected in coincidence with a highly converted transition at 50 keV. This decay pattern has strong similarities with that seen in the neighboring ^{243,245,251}Es isotopes [23], where the $9/2^+$ member of the signature partner rotational band built on the $7/2^+$ is fed by an $E1$ transition. The transition rate for a decay from a

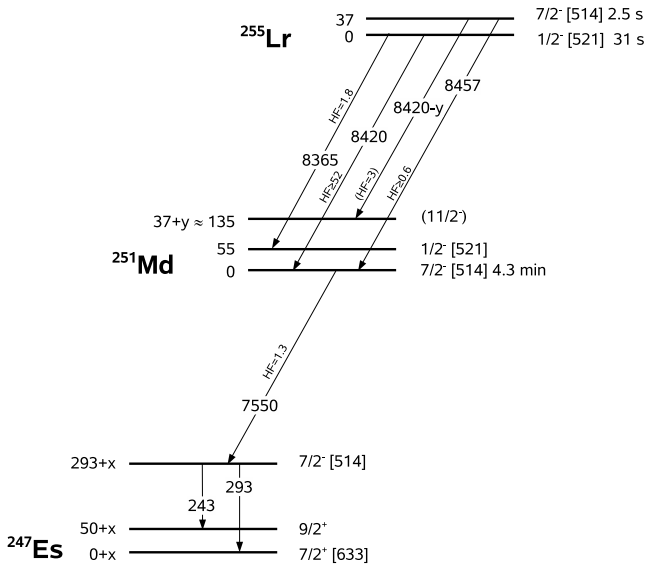

Fig. 13. Level scheme of ^{247}Es ^{251}Md and ^{255}Lr deduced from experimental data. The tentative 8290 keV line from ^{255}Lr is not shown.

I_1, K_1 to a I_2, K_2 rotational state can be estimated using the Alaga rule [50]. For $E\lambda$ transitions, the expression is:

$$T(E\lambda) \propto E^{2\lambda+1} \langle I_1 \;\; K_1 \;\; \lambda \;\; K_2 - K_1 | I_2 \;\; K_2 \rangle^2. \quad (5)$$

The calculation leads to an intensity ratio $T(E1,293)/T(E1,243) = 6.1$ compared to $T(E1,293)/T(E2,243) = 212$. The experimental value of 4.4 ± 2 supports therefore an $E1$ assignment for both transitions, 243 and 293 keV. Consequently, the highly converted 50 keV transition summed with the 7550 keV α line corresponds to the $M1$ transition between $9/2^+$ and $7/2^+$ states. The 7550 keV α-decay to the $7/2^-$ state of ^{247}Es at 293 keV has an hindrance factor of 1.3, which strongly suggests that the single-particle configuration is the same for the initial and final states. It follows that the initial state, which is the ground state of ^{251}Md, has a spin and parity of $7/2^-$.

No candidate α-decays from ^{251}Md for the transition to the predicted $3/2^-$ state were observed in the present data. It should be noted that due to the spin-flip nature of the $7/2^-[514] \rightarrow 3/2^-[521]$ transition, such a decay would be strongly hindered. The position of the $3/2^-$ state therefore remains unknown and the ground-state spin and parity of ^{247}Es remains uncertain. The deduced experimental level scheme of ^{247}Es is shown in fig. 13.

5.2 ^{251}Md and ^{255}Lr

The α-decays of ^{255}Lr at 8365 and 8457 keV energies have a small hindrance factor, and should each connect configurations corresponding to the same one–quasi-particle level. Since two α-decays of the ^{255}Lr ground state, at 8365 and 8420 keV, have been detected, the 8365 keV decay cannot feed the ^{251}Md ground state. It is therefore the 8457 keV transition from the 2.53 s isomeric state which feeds the $7/2^-$ ^{251}Md ground state. According to the hindrance factor value, the isomeric state in ^{255}Lr has the same spin and parity as the ^{251}Md ground state, $7/2^-$. The HFB calculations predict a $7/2^-$ ground state for ^{255}Lr and only two excited states below 400 keV: $1/2^-$ and $7/2^+$. Since there is an uncertainty of a few hundred keV in the theory, both the $1/2^-$ and the $7/2^+$ configurations could correspond to the ^{255}Lr ground state. The ground state $7/2^+$ can be easily ruled out: the $7/2^-$ state would then decay by an $E1$ transition and would not be isomeric. The only possibility for the ^{255}Lr ground state is therefore a spin and parity of $1/2^-$, in which case the $7/2^-$ state decays to the $1/2^-$ state by a $M3$ transition and is isomeric. The ^{255}Lr ground state decays by the 8365 keV transition to an excited ^{251}Md level with the same spin and parity ($1/2^-$). A rotational band built on the $1/2^-$ state in ^{251}Md has been recently observed [15] which confirms the presence of such a state at low excitation energy. The 8420 keV transition from the ^{255}Lr ground state has a large hindrance factor of ≥ 52, compatible with an $1/2^- \rightarrow 7/2^-$ transition.

The two transitions from the ^{255}Lr ground state allow us to determine the excitation energy of the $1/2^-$ state in ^{251}Md to be around 55 keV. The isomeric $7/2^-$ state in ^{255}Lr then has an excitation energy of 37 keV. The Weisskopf estimate for the lifetime of a 37 keV $M3$ transition is 0.3 s, compatible with the experimental half-life of 2.53 s for the isomeric state.

The α line at 8420 keV from the isomeric state in ^{255}Lr is compatible with the feeding of an excited state in ^{251}Md. Using the same arguments as in sect. 4.1, the excited state should decay via a fully converted transition and the subsequent X-ray, Coster-Kronig and Auger electron should sum with the coincident α line. Therefore, the measured 4820 keV energy should not correspond to the α-decay energy. Sequences of alpha-decays feeding states at I_f, $I_f + 1$, $I_f + 2$ have been observed in several transuranium isotopes (see for instance [41]), with intensity ratios $I(I_i \rightarrow I_f)/I(I_i \rightarrow I_f + 1) \sim 2$–3 and $I(I_i \rightarrow I_f)/I(I_i \rightarrow I_f + 2) \sim 10$. Let us consider the feeding of the $9/2^-$ rotational state at an energy of $\sim$ 50 keV (assuming a 75 $\hbar^2$ MeV^{-1} moment of inertia). From GEANT 4 simulations, the 50 keV $M1$ transition leads to a summing of $\sim$ 41 keV with 8457-50 keV resulting in a 8448 keV α line. Such a line should lie in the tail of the 8457 transition and cannot be resolved. The $11/2^-$ rotational state at an energy of $\sim$ 135 keV should decay via two $M1$ transitions at $\sim$ 85 and $\sim$ 50 keV. Indeed, transition rates reported in [15] do not favour the $E2$ ($11/2^- \rightarrow 7/2^-$) transition. The two $M1$ transitions should again sum with the α line at 8457-85-50 = 8322 keV. GEANT 4 simulations suggest a broad line at $\sim$ 8430 keV which is compatible with the 8420 ± 10 keV peak (remember also that the GEANT 4 simulations presented in sect. 4.1 overestimate the experimental summing effect). We observe here an intensity ratio $I(8457)/I(8420) \sim 12$ which is compatible with the feeding of the $7/2^- + 2 = 11/2^-$ rotational state. We therefore interpret the 8420 line as a broad summed peak corre-

sponding to the feeding of a $11/2^-$ state at ~ 135 keV excitation energy. The 8457 keV peak should also correspond to an unresolved doublet including the $7/2^- \rightarrow 7/2^-$ transition and the $7/2^- \rightarrow 9/2^-$ summed line. The hindrance factor for the 8457 line should be therefore considered as a lower limit.

Finally, coincidences between the 8290 keV α and 75 ± 10 keV electron lines are tentatively observed, suggesting the feeding of a state at above 130 keV excitation energy.

The $7/2^+$ state, predicted in both ^{251}Md and ^{255}Lr, has not been observed: the α transition feeding or deexciting this state involves a change in parity and therefore, would be strongly hindered. One can also expect the $1/2^-$ ^{251}Md state to be isomeric. The $M3$ transitions in ^{255}Lr and ^{251}Md should both be similar and the 55 keV level of ^{251}Md should have *a priori* a lifetime of a few seconds. As a consequence, the decay curve of the 7550 keV α line should show the characteristic features of a two-step process. However, a few seconds is a short time compared to 4.3 minutes and the distortion of the decay curve should be very small. Moreover, an $1/2^- \rightarrow 1/2^-$ α transition feeding ^{247}Es would also be expected, having an hindrance factor close to one, similar to that observed in the decay of ^{255}Lr. Assuming that the $1/2^-$ state in ^{251}Md has a lifetime between 2 and 5 s, the α-decay branching ratio for the ^{251}Md$(1/2^-) \rightarrow {}^{247}Es(1/2^-)$ transition should be less than 1%. This is well below the detection limit. It remains likely, however, that the $1/2^-$ state in ^{251}Md is isomeric. The level schemes resulting from all these considerations are shown in fig. 13.

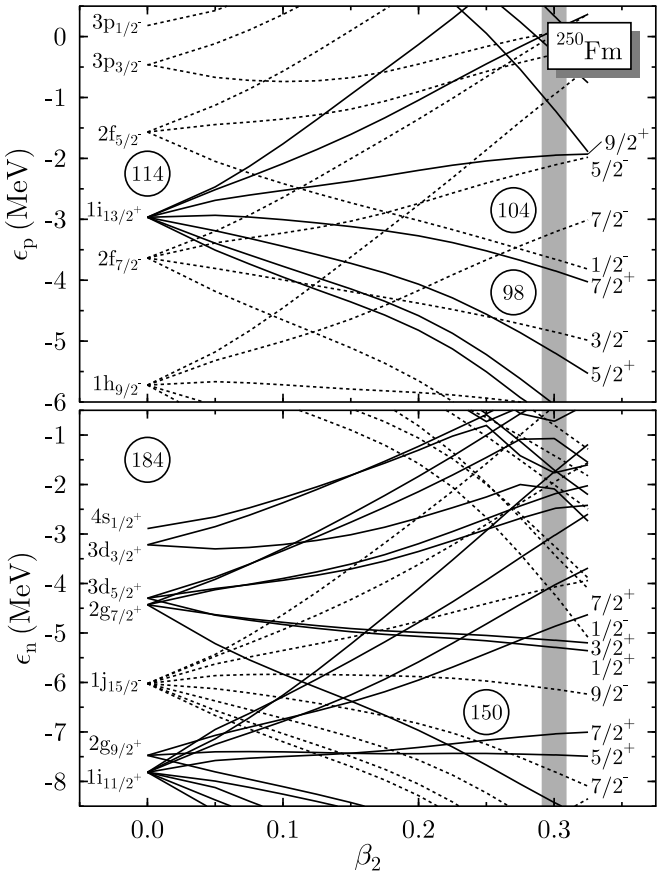

Fig. 14. Single-particle spectra of ^{250}Fm for protons (top) and neutrons (bottom) obtained with the SLy4 interaction. The vertical grey bar indicates the range of ground-state deformations predicted for this and neighboring nuclei.

6 Discussion

In this section the single-particle structure of the odd-Z Es, Md and Lr isotopes deduced from experiment is discussed and compared to the HFB calculations.

6.1 Es isotopes

Energy level systematics of the Es isotopes deduced from experimental data are shown in the lower part of fig. 15. Extensive discussion of the Es level systematics can be found in [23]. Very similar γ-ray transitions between $7/2^-$ and $7/2^+$ states have been observed in ^{243}Es [23], ^{245}Es [23], ^{247}Es (this work), ^{249}Es [51,23], ^{251}Es [52,43, 53] and ^{253}Es [54]. In ^{243,245,247,251,253}Es, the decay from the $7/2^-$ to the $9/2^+$ rotational state has also been observed. The relative position of the $7/2^-$ and $7/2^+$ states increases up to ^{251}Es and then decreases. It is interesting to note that this may be related to evolution of deformation, which should reach a maximum at the $N = 152$ deformed shell gap. As a consequence, the distance between the up-sloping $7/2^-$ and the down-sloping $7/2^+$ orbitals increases due to the increase of deformation as can be seen on the proton single-particle spectrum in the upper part of fig. 14. This trend is rather well reproduced by theory as shown in the middle part of fig. 15. However, HFB calculations using the SLy4 interaction underestimate the $N = 152$ (^{251}Es) deformed shell gap and favour $N = 150$ as deformed magic number. This appears clearly in the lower part of fig. 14. The β_2 deformation parameter for the states corresponding to different quasi-particle excitations is shown in the upper part of fig. 15. We have displayed with solid lines the deformation parameter deduced from the charge quadrupole moment defined as

$$\beta_2^p = \sqrt{\frac{5}{16\pi}} \frac{4\pi}{3R^2 Z} Q_2^p, \tag{6}$$

taking $R = 1.2A^{1/3}$ fm. The proton deformation is almost the same for all states. However, the deformation driving polarisation effect of the down-sloping Nilsson orbitals $1/2^-[521]$ and $7/2^+[633]$ located above the Fermi level is still clearly seen. For comparison, we have also calculated the deformation parameter deduced from the quadrupole moment of the neutrons defined as

$$\beta_2^n = \sqrt{\frac{5}{16\pi}} \frac{4\pi}{3R^2 N} Q_2^n. \tag{7}$$

The β_2^n parameter for the ground state is displayed with a dotted line. This curve shows the neutron-driving deformation effect which is maximum for $N = 150$. The proton

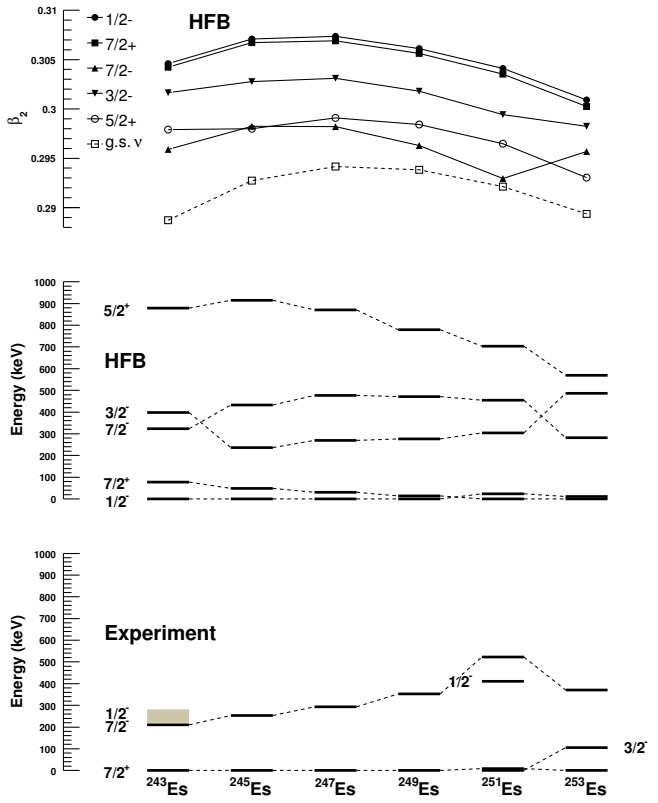

Fig. 15. Systematics of the one–quasi-particle states in the Es isotopes. Skyrme-HFB calculations are performed using the Skyrme interaction SLy4 and a density-dependent pairing interaction. Top panel: β_2 deformation parameter extracted from protons (solid lines for the different quasi-particle states) or neutrons (dotted line for the ground state) quadrupole moment. Middle panel: quasi-particle states energies; lower panel: experimental data. The $3/2^-$ state has not been observed in $^{243-249}$Es, and could correspond to the ground state.

β_2^p deformation is systematically larger than the neutron one. We have checked that this effect is not an artefact due to the β_2 parametrization. A plausible explanation of the difference between proton and neutron β_2 deformations is that it is due to the Coulomb repulsion which drives protons to more elongated shapes. One can also note that Skyrme-HFB calculations predict a very smooth evolution of the $7/2^-$ excitation energy in Es isotopes, whereas experimental data show a marked maximum at $N = 152$.

The calculation over-predicts the separation between the $7/2^-$ and $7/2^+$ states by approximately 200 keV, which is well within the theoretical uncertainties. A $3/2^-$ state has not been observed in ^{247}Es in the present work. As explained in sect. 5.1, the α-decay from ^{251}Md to the $3/2^-$ state of ^{247}Es, along with electromagnetic transitions from or to this state, is not favored. In ref. [49], a ground-state spin and parity of $3/2^-$ ($7/2^+$) is proposed for ^{243,245}Es (^{247,249}Es). As was pointed out in [6, 23], this assignment is ambiguous and the ground-state spin and parity for these 4 isotopes are uncertain. Detailed data for ^{251}Es were obtained in [52,43], where the ground state is assigned to be $3/2^-$. A very robust assignment of $7/2^+$ to the ground state of ^{253}Es has been obtained using optical spectroscopy [55]. Experimental data indicate therefore that the $7/2^+$ and $3/2^-$ states lie very close in energy in the Es isotopes. Theoretically, our calculations predict a decrease of the $3/2^-$ excitation energy from ^{251}Es to ^{245}Es. Lowering the calculated $3/2^-$ level by around 300 keV would reproduce the experimental data in ^{251,253}Es very well, and would predict a $3/2^-$ ground state in $^{245-249}$Es. However, a general trend as a function of the deformation cannot be easily drawn since both $3/2^-$ and $7/2^+$ orbitals are down-sloping as a function of the quadrupole deformation: see the upper part of fig. 14.

The possibility for the presence of the $1/2^-$ state has been reported in ^{243}Es above the $7/2^-$ state [56]. It has also been observed in ^{251}Es at 411 keV [52,43]. The position of the $1/2^-$ state in the Es, Md and Lr isotopes will be discussed in sect. 6.4.

6.2 Md isotopes

Less detailed experimental data have been obtained for the Md isotopes. A $7/2^-$ ground state has been assigned to ^{247}Md [23,56], ^{249}Md [23,57] and ^{251}Md (this work). In ^{253}Md, evaluated data [22] based on α-decay studies [38] suggest a $1/2^-$ ground state. Recent experiments [23] show instead that ^{253}Md has a $7/2^-$ ground state. The ground state of ^{255}Md has been assigned to be $7/2^-$ through the study of electron capture and α-decay [43]. In ^{247,249,251}Md, the $1/2^-$ level is proposed as the first excited single-particle state. Its position is not reproduced by our HFB calculations, which predict a $1/2^-$ ground state for the isotopes $^{245-255}$Md and put the $7/2^-$ state at small excitation energy between 100 and 200 keV. The calculations also predict a $7/2^+$ state in the same energy range, which has not been observed in the Md isotopes since its feeding through α-decay from ^{255}Lr $1/2^-$ or $7/2^-$ is hindered. Results of Skyrme-HFB calculations for the $^{245-257}$Md isotopes are shown in fig. 16.

6.3 Lr isotopes

To deduce the level structure of Lr isotopes from α-decay studies requires either the knowledge of the Md daughter nucleus, or α-decay data from the mother Db isotope. Both data are still scarce and little has been deduced from experiment. Besides the present study of ^{255}Lr, a ground state of $7/2^-$ has been deduced in ^{253}Lr [57], with a $1/2^-$ excited state the energy of which could not be determined. As isomeric states may not have been observed in some experiments, the $7/2^-$ ground-state assignment of ^{257}Lr [22] should be taken with care. The position of the $1/2^-$ and $7/2^-$ states is known for the ^{253,255}Lr isotopes only. The two states have been observed to be very close in energy, with an inversion between these two isotopes. However, theory predicts a $7/2^-$ ground state for the two isotopes (see fig. 17) having a very similar deformation.

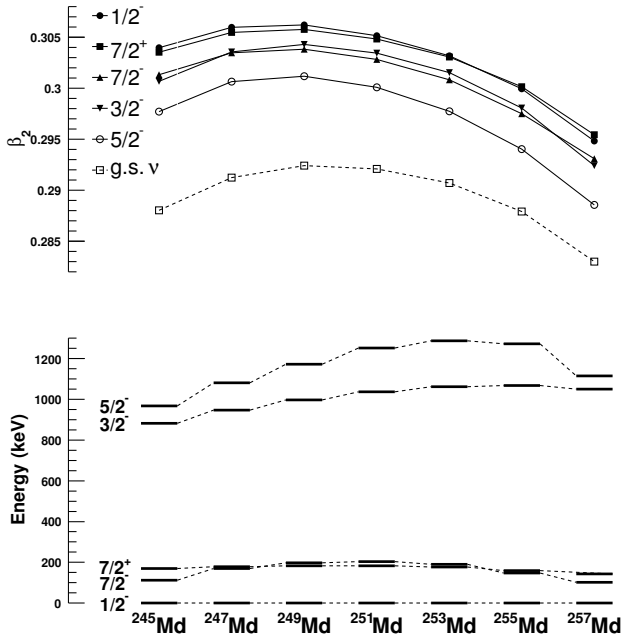

Fig. 16. Skyrme-HFB calculations for the Md isotopes. Top panel: β_2 deformation parameter (see fig. 15 for explanations). Lower panel: one–quasi-particle states.

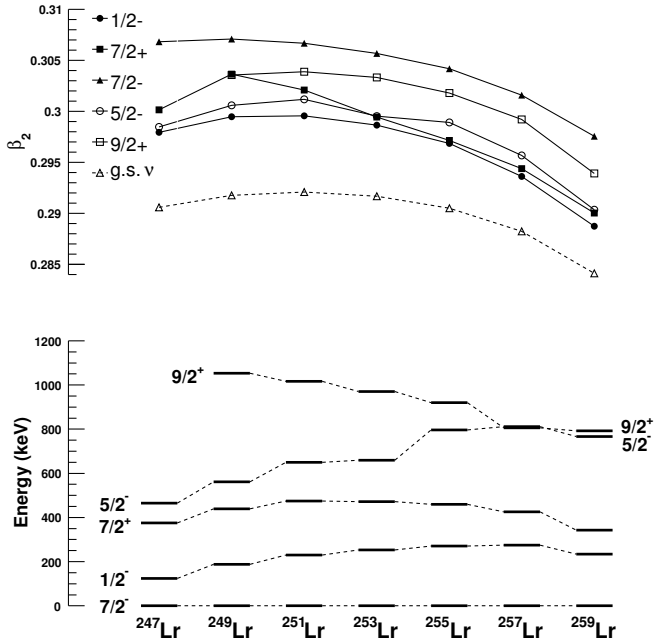

Fig. 17. Skyrme-HFB calculations for the Lr isotopes. Top panel: β_2 deformation parameter (see fig. 15 for explanations). Lower panel: one–quasi-particle states.

Assuming a lowering of the $1/2^-$ orbital, any small deformation changes could swap the two states. Note also that all theories fail to reproduce the $1/2^-$ ground-state spin of ^{255}Lr [46,48,47]. HFB calculations for $^{247-259}$Lr are shown in fig. 17.

6.4 The $1/2^-$ state and the $2f_{5/2}$ shell

As mentioned above, the trend for the $7/2^+$ and $7/2^-$ states is well reproduced by the Skyrme-HFB calculation. The most striking disagreement concerns the position of the $1/2^-$ state, predicted to be the ground state of Es and Md isotopes, while it is observed as an excited state in ^{243,251}Es and ^{247,249,251}Md.

Beyond this ascertainment, it should be pointed out that, experimentally, the $7/2^-$ and $1/2^-$ levels always lie very close in energy. This effect could be due to an over-estimation of deformation since the $1/2^-$ orbital is down-sloping whilst the $7/2^-$ orbital is up-sloping: see the upper part of fig. 14. However, HFB calculations with SLy4 interaction using the same formalism [58] reproduce very well the moment of inertia of the even-even ^{252,254}No isotopes, which makes this hypothesis unlikely. Another source of error could be the separation between the different shells at sphericity. In the Es isotopes, states corresponding to quasi-particle excitations of orbitals from 4 different spherical shells have been observed: $1/2^-$ ($2f_{5/2}$), $7/2^-$ ($1h_{9/2}$), $7/2^+$ ($1i_{13/2}$) and $3/2^-$ ($2f_{7/2}$). The close position of the $7/2^-$ and $1/2^-$ levels in all Es, Md and Lr isotopes studied so far seems to indicate an underestimation of the distance between the $2f_{5/2}$ and $1h_{9/2}$ spherical shells by about 200 keV. The close position of the $3/2^-$ and $7/2^+$ states in ^{251,253}Es suggests also that the $2f_{7/2}$ spherical shell should be pushed up by about 700 keV. On the other hand, the relative position of the $1h_{9/2}$ ($7/2^-$) and $1i_{13/2}$ ($7/2^+$) seems to be correct. These hypotheses go along the same lines as the discussion in ref. [45], which suggests a lowering of the separation between the $2f_{5/2}$ and $2f_{7/2}$ shells.

As the down-sloping $1/2^-$ and up-sloping $7/2^+$ states are very close in energy, the inversion of these levels seen between ^{253}Lr and ^{255}Lr is not of great significance within our scenario: any small modification of the effective interaction, inducing a small change in deformation or pairing correlations, could change the relative position of the two levels.

There is a long-standing prediction from microscopic-macroscopic models of $Z = 114$ being the next proton shell closure [59–62]. The appearance and size of the $Z = 114$ gap depends on the relative position of the $2f$ and $1i_{13/2}$ levels, and, in particular, the spin-orbit splitting of the $2f$ states, which enclose the $Z = 114$ gap. All standard microscopic-macroscopic models place the $1i_{13/2}$ level below the $2f_{7/2}$ one and give a large spin-orbit splitting of the $2f$ levels. The resulting prediction of a major $Z = 114$ shell closure, however, is not confirmed by modern self-consistent mean-field models [2,4] as for example the Skyrme interaction SLy4 that we use here. Most of these models push the $1i_{13/2}$ level between the $2f$ states, as can be seen in fig. 14, or reduce the spin-orbit splitting of the $2f$ states, or both. Furthermore, it has been pointed out that even with their already reduced spin-orbit splittings, all mean-field models still tend to overestimate the spin-orbit splittings in heavy nuclei, as for example ^{208}Pb [2], which hints that the spin-orbit split-

ting of the $2f$ states should be even smaller than the values predicted by SLy4.

The relative shifts of single-particle levels suggested above can be confronted with this scenario for HFB calculation using the Skyrme interaction SLy4. When using the well-described distance of the $1h_{9/2}$ and $1i_{13/2}$ levels as a reference, then the splitting between the $2f$ levels should indeed be reduced by about 500 keV. At the same time, the centroid of the $2f$ levels should be shifted relative to the $1i_{13/2}$ level such that the $1i_{13/2}$ and $2f_{7/2}$ levels will be nearly degenerate, while the $Z = 114$ gap slightly opens up between the $1i_{13/2}$ and $2f_{5/2}$ levels, but remains too small to establish a major shell closure.

7 Summary and conclusion

The fusion-evaporation reaction of ^{48}Ca + ^{209}Bi was used to study ^{255}Lr, and via successive α-decays the odd-Z transfermium nuclei ^{251}Md and ^{247}Es. Alpha, γ and electron spectroscopy were used to probe single-particle properties around the doubly magic deformed shell gap at $Z = 100$, $N = 152$. A revised half-life of 31.1 ± 1.3 s was measured for the $1/2^-$ ground state of ^{255}Lr, and the analysis revealed a new isomeric $7/2^-$ state in ^{255m}Lr with a half-life of 2.53 ± 0.13 s. The improved α-decay data allowed the energies of excited states in ^{251}Md to be determined. New γ-ray transitions in ^{247}Es were observed, which allowed a level scheme for the latter to be proposed. As a consequence, the Q_α values for ^{255}Lr should be revised, for the ground-state–to–ground-state decay a value of 8554 ± 10 keV is determined. For ^{251}Md, the ^{247}Es ground state may not have been observed. Therefore, only a lower limit of 7970 keV can be given. For comparison, the values given in the AME2003 evaluation [63] are 7990 ± 200 keV for ^{251}Md and 8610 ± 30 keV for ^{255}Lr.

The spin and parities of ground and excited states were deduced using γ-ray transitions and their multipolarities and α-decay energies and hindrance factors. Nilsson labels have been assigned to the observed states: $7/2^+[633]$ either as an excited or the ground state of ^{247}Es; $7/2^-[514]$ as an excited state of ^{247}Es, ^{255}Lr and the ground state of ^{251}Md. $1/2^-[521]$ is deduced as the ground state of ^{255}Lr and as an excited state of ^{251}Md. The agreement with HFB calculations using the Skyrme interaction SLy4 is satisfactory for the $7/2^-$ and $7/2^+$ states. On the other hand, the position of the $1/2^-[521]$ down-sloping orbital from the spherical $2f_{5/2}$ shell is not well reproduced by the HFB calculations. Note that the models fail in general to predict a $1/2^-$ character for the ground state of ^{255}Lr. The proximity to the $7/2^-$ state, also established in neighbouring Es and Md isotopes suggests a slightly underestimated position of the $2f_{5/2}$ shell.

Our experimental results provide new conclusive results in the region of the heaviest actinides. The combination of α, γ, and electron spectroscopy combined with separators with high-beam rejection was decisive in establishing the single-particle structure of ^{255}Lr, ^{251}Md and ^{247}Es. Many ambiguities remain, however, for some of the heaviest elements, both in odd-Z and odd-N nuclei. In the light of this study, it is clear that some elements should be revisited and studied in more detail to address these ambiguities.

We are grateful to the University of Jyväskylä and GANIL for their excellent technical support. We are greatly indebted to P. Bourgault, G. Frémont and Ch. Spitaels from GANIL for building BEST and making ^{209}Bi targets. Very fruitful discussions with T. Duguet are greatly acknowledged. We are grateful to M.M. Bé (Laboratoire National Henri Becquerel) and Ch. Bonnelle (Université Pierre et Marie Curie, Paris VI) for helpful discussions on atomic processes. This work has been supported by the European Union Fifth Framework Programme "Improving Human Potential - Access to Research Infrastructure" Contract No. HPRI-CT-1999-00044 and by the Academy of Finland under the Finnish Centre of Excellence Programme 2000-2005 (Project No. 44875, Nuclear and Condensed Matter Physics Programme at JYFL). Ch.T. acknowledges the warm hospitality of GANIL for a sabbatical period during which BEST was built.

References

1. S. Hofmann, G. Münzenberg, Rev. Mod. Phys. **72**, 733 (2000).
2. M. Bender, K. Rutz, P.-G. Reinhard, J.A. Maruhn, W. Greiner, Phys. Rev. C **60**, 034304 (1999).
3. M. Bender, P.-H. Heenen, P.-G. Reinhard, Rev. Mod. Phys. **75**, 121 (2003).
4. A.T. Kruppa, M. Bender, W. Nazarewicz, P.-G. Reinhard, T. Vertse, S. Ćwiok, Phys. Rev. C **61**, 034313 (2000).
5. R.-D. Herzberg, J. Phys. G **30**, R123 (2004).
6. M. Leino, F.P. Hessberger, Annu. Rev. Nucl. Part. Sci. **54**, 175 (2004).
7. P. Reiter *et al.*, Phys. Rev. Lett. **82**, 509 (1999).
8. M. Leino *et al.*, Eur. Phys. J. A **6**, 63 (1999).
9. S. Eeckhaudt *et al.*, Eur. Phys. J. A **26**, 227 (2005).
10. P.A. Butler *et al.*, Phys. Rev. Lett. **89**, 202501 (2002).
11. R.-D. Herzberg *et al.*, Nature **442**, 896 (2006).
12. S.K. Tandel *et al.*, Phys. Rev. Lett. **97**, 082502 (2006).
13. J.E. Bastin *et al.*, Phys. Rev. C **73**, 024308 (2006).
14. R.-D. Herzberg *et al.*, Phys. Rev. C **65**, 014303 (2002).
15. A. Chatillon *et al.*, PhD Thesis, Université Lyon I - Claude Bernard (2006).
16. P. Reiter *et al.*, Phys. Rev. Lett. **95**, 032501 (2005).
17. R.-D. Herzberg *et al.*, Eur. Phys. J. A **15**, 205 (2002).
18. P.T. Greenlees *et al.*, private communication.
19. R.D. Page *et al.*, Nucl. Instrum. Methods B **204**, 634 (2003).
20. K. Hauschild *et al.*, Nucl. Instrum. Methods A **560**, 388 (2006).
21. P. Eskola, Phys. Rev. C **7**, 280 (1973).
22. A. Artna-Cohen, Nucl. Data Sheets **88**, 155 (1999).
23. F.P. Hessberger *et al.*, Eur. Phys. J. A **26**, 233 (2005).
24. H.W. Gäggler *et al.*, Nucl. Phys. A **502**, 561c (1989).
25. M. Leino *et al.*, Nucl. Instrum. Methods B **99**, 653 (1995).
26. I.H. Lazarus *et al.*, IEEE Trans. Nucl. Sci. **48**, 567 (2001).
27. P. Rahkila *et al.*, unpublished.
28. R. Anne, D. Bazin, A.C. Mueller, J.C. Jacmart, M. Langevin, Nucl. Instrum. Methods A **257**, 215 (1987).
29. S. Grévy *et al.*, J. Nucl. Radiat. Sci. **4**, 1 (2002).

30. R. Anne, A.C. Mueller, Nucl. Instrum. Methods B **70**, 276 (1992).
31. F. Méot, S. Valéro, SATURNE Note LNS/GT/93-12.
32. K. Makino, M. Berz, Nucl. Instrum. Methods A **427**, 338 (1999).
33. S. Agostinelli *et al.*, Nucl. Instrum. Methods A **506**, 250 (2003).
34. J. Simpson *et al.*, Acta. Phys. Hung. N.S. - Heavy Ion Phys. **11**, 159 (2000).
35. R. Brun, F. Rademakers, Nucl. Instrum. Methods A **389**, 81 (1997). See also `http://root.cern.ch/`.
36. M. Leino, S. Yashita, A. Ghiorso, Phys. Rev. C **24**, 2370 (1981).
37. K. Eskola, P. Eskola, M. Nurmia, A. Ghiorso, Phys. Rev. C **4**, 632 (1971).
38. C.E. Bemis *et al.*, report ORNL-5137 (1976) p. 73; ORNL-5111 (1976) p. 58.
39. M.A. Preston, Phys. Rev. **71**, 865 (1947).
40. J.O. Rasmussen, *Alpha-, Beta- and Gamma-Ray Spectroscopy*, edited by K. Siegbahn, Vol. **1** (North-Holland, Amsterdam, 1955) Chapt. XI, p. 701.
41. R.B. Firestone, V.S. Shirley *et al.*, *Table of Isotopes*, eighth edition (John Wiley & Sons, Inc., 1998).
42. A. Lopez-Martens *et al.*, Phys. Rev. C **74**, 044303 (2006).
43. I. Ahmad, R.R. Chasman, P.R. Fields, Phys. Rev. C **61**, 044301 (2000).
44. E. Chabanat, P. Bonche, P. Haensel, J. Meyer, R. Schaeffer, Nucl. Phys. A **635**, 231 (1998).
45. M. Bender, P. Bonche, T. Duguet, P.-H. Heenen, Nucl. Phys. A **723**, 354 (2003).
46. S. Ćwiok, S. Hofmann, W. Nazarewicz, Nucl. Phys. A **573**, 356 (1994).
47. A. Parkhomenko, A. Sobiczewski, Acta Phys. Pol. B **35**, 2447 (2004).
48. H. Goutte, private communication.
49. Y. Hatsukawa *et al.*, Nucl. Phys. A **500**, 90 (1989).
50. G. Alaga, K. Alder, A. Bohr, B.R. Mottelson, Mat.-Fys. Medd. K. Dan. Vidensk. Selsk. **29**, no. 9, 1 (1955).
51. I. Ahmad, R.K. Sjoblom, R.F. Barnes, E.P. Horwitz, P.R. Fields, Nucl. Phys. A **140**, 141 (1970).
52. I. Ahmad, R.K. Sjoblom, A.M. Friedman, S.W. Yates, Phys. Rev. C **17**, 2163 (1978).
53. I. Ahmad, A.M. Friedman, R.R. Chasman, S.W. Yates, Phys. Rev. Lett. **39**, 12 (1977).
54. K.J. Moody *et al.*, Nucl. Phys. A **563**, 21 (1993).
55. E.F. Worden, R.G. Gutmacher, R.W. Lougheed, J.E. Evans, J.G. Conway, J. Opt. Soc. Am. **58**, 998 (1968); E.F. Worden, R.G. Gutmacher, R.W. Lougheed, J.G. Conway, R.J. Mehlhorn, J. Opt. Soc. Am. **60**, 1297 (1970).
56. F.P. Hessberger *et al.*, GSI Scientific Report, GSI 2003, 2004-1 (2004) p. 3.
57. F.P. Hessberger *et al.*, Eur. Phys. J. A **12**, 57 (2001).
58. T. Duguet, P. Bonche, P.-H. Heenen. Nucl. Phys. A **679**, 427 (2001).
59. W.D. Myers, W.J. Swiatecki, Nucl. Phys. **81**, 1 (1966).
60. A. Sobiczewski, F.A. Gareev, B.N. Kalinkin, Phys. Lett. **22**, 500 (1966).
61. H. Meldner, Ark. Fys. **36**, 593 (1967).
62. H. Meldner, Phys. Rev. **178**, 1815 (1969).
63. G. Audi, A.H. Wapstra, C. Thibault, Nucl. Phys. A **729**, 337 (2003).